Journal of Magnetic Resonance 211 (2011) 134–142

Contents lists available at ScienceDirect

Journal of Magnetic Resonance

journal homepage: www.elsevier.com/locate/jmr

Investigation of the effect of a variety of pulse errors on spin $I = 1$ quadrupolar alignment echo spectroscopy

Xiang Ma, Cheng Sun, Gregory S. Boutis *

Brooklyn College, Department of Physics, 2900 Bedford Avenue, Brooklyn, NY 11210, United States

ARTICLE INFO

Article history:
Received 14 February 2011
Revised 22 April 2011
Available online 18 May 2011

Keywords:
Quadrupolar relaxation
Quadrupolar interaction
Multiple quantum filtering
T_{1Q}

ABSTRACT

We report on an analysis of a well known three-pulse sequence for generating and detecting spin $I = 1$ quadrupolar order when various pulse errors are taken into account. In the situation of a single quadrupolar frequency, such as the case found in a single crystal, we studied the potential leakage of single and/or double quantum coherence when a pulse flip error, finite pulse width effect, RF transient or a resonance offset is present. Our analysis demonstrates that the four-step phase cycling scheme studied is robust in suppressing unwanted double and single quantum coherence as well as Zeeman order that arise from the experimental artifacts, allowing for an unbiased measurement of the quadrupolar alignment relaxation time, T_{1Q}. This work also reports on distortions in quadrupolar alignment echo spectra in the presence of experimental artifacts in the situation of a powdered sample, by simulation. Using our simulation tool, it is demonstrated that the spectral distortions associated with the pulse artifacts may be minimized, to some extent, by optimally choosing the time between the first two pulses. We highlight experimental results acquired on perdeuterated hexamethylbenzene and polyethylene that demonstrate the efficacy of the phase cycling scheme for suppressing unwanted quantum coherence when measuring T_{1Q}. It is suggested that one employ two separate pulse sequences when measuring T_{1Q} to properly analyze the short time behavior of quadrupolar alignment relaxation data.

1. Introduction

Deuteron quadrupolar alignment echo spectroscopy is a powerful tool for probing molecular motions with relaxation times in the range of T_2^* to T_1, corresponding to a correlation time of 10^{-5} s and greater [1,2]. The method has been successfully applied to study structure and dynamics in a wide range of systems of interest in polymer and chemical physics, biophysics and materials science. Two of the earliest works in the field that implemented the approach involved a study of molecular dynamics in liquid crystals [3] and motional constraints in polyethylene [1,2]. The approach has been used to study slow tetrahedral jumps in solid hexamethylenetetramine [4], the dynamics of gramicidin [5], to investigate the localized dynamics in DNA fragments [6], and more recently hydration dependent dynamics in RNA [7].

The pulse sequence for generating and detecting quadrupolar order consists of three pulses with shifted phases as shown in Fig. 1. Quadrupolar order is excited by the second pulse, evolves during the delay T and is subsequently converted into an observable signal by the last pulse. By varying T, the relaxation time of quadrupolar order, T_{1Q}, can be measured. This pulse sequence intrinsically generates quadrupolar order and double quantum coherence at the same time even under ideal experimental conditions [3]. The unwanted double quantum coherence can be readily suppressed from the detected signal by phase cycling [3].

One of the prerequisites for performing T_{1Q} experiments on rigid solids is the use of high RF power to excite the nuclear spin ensemble bandwidth, which may exceed 100 kHz. The use of high RF power inevitably introduces a variety of pulse artifacts, such as phase transients. Other unavoidable experimental errors include a flip angle error, finite pulse width effect and off-resonance artifact. It is well known from the coherence pathway formalism, that perfect spin rotations as well as the pulse and receiver phase are crucial for the selection of certain orders of quantum coherence [8]. Jerschow has reported on a spherical tensor based formalism that quantifies the effects of imperfect rotations when selecting a quantum coherence of interest [9]. In this work, we studied the effects of pulse errors on the alignment echo three-pulse sequence via the fictitious spin-$\frac{1}{2}$ operators developed by Vega and Pines [10]. For the case that only one quadrupolar frequency, ω_Q, is present in the spin ensemble (as is the case for a single crystal, for example), we investigated the potential leakage of multiple quantum coherence due to pulse errors. The results show that a simple four-step phase cycling scheme is robust for selecting quadrupolar order if the errors are small, though the signal intensity may be reduced. For the case of a powder distribution of ω_Q, we simulated the quadrupolar alignment echo spectra and demonstrated that finite

* Corresponding author. Fax: +1 718 951 4407.
E-mail address: gboutis@brooklyn.cuny.edu (G.S. Boutis).

1090-7807/$ - see front matter © 2011 Elsevier Inc. All rights reserved.
doi:10.1016/j.jmr.2011.05.003

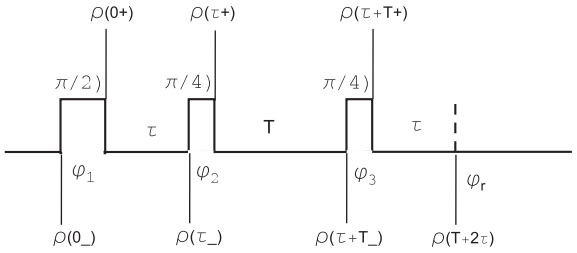

Fig. 1. A three pulse sequence for generating and detecting quadrupolar order. In the figure, the phases ϕ_1, ϕ_2, ϕ_3 and ϕ_r refer to the RF phases and receiver phase tabulated in Table 1.

pulse width effects, phase transients and pulse flip errors all distort the powder line shape but that the distortions may be minimized to some degree by a judicious choice of spacing between the first two pulses. Lastly, we highlight experimental data on perdeuterated hexamethylbenzene and polyethylene that demonstrate the effectiveness of a simple four-step phase cycling scheme that was investigated. It is suggested that one perform two experiments with two different phase cycles to verify that the short time behavior of the quadrupolar alignment relaxation data does not include accidentally leaked double quantum coherence.

2. Case I: Theoretical treatment for the case of a single quadrupolar frequency

The fictitious spin-$\frac{1}{2}$ operators were introduced by Vega and Pines to conveniently describe the interaction of a spin $I = 1$ nucleus with a Radio Frequency (RF) field [10]. In this formalism, the basis consists of nine operators given by

$$\begin{aligned} I_{x,1} &= \frac{1}{2}I_x, \quad I_{x,2} = \frac{1}{2}(I_yI_z + I_zI_y), \quad I_{x,3} = \frac{1}{2}\left(I_z^2 - I_y^2\right) \\ I_{y,1} &= \frac{1}{2}I_y, \quad I_{y,2} = \frac{1}{2}(I_zI_x + I_xI_z), \quad I_{y,3} = \frac{1}{2}\left(I_x^2 - I_z^2\right) \\ I_{z,1} &= \frac{1}{2}I_z, \quad I_{z,2} = \frac{1}{2}(I_xI_y + I_yI_x), \quad I_{z,3} = \frac{1}{2}\left(I_y^2 - I_x^2\right) \end{aligned} \tag{1}$$

From these definitions the various orders of multiple quantum coherence are as follows

$$\begin{aligned} I_{x,1}, I_{y,1}, I_{x,2}, I_{y,2} &: \text{single quantum} \\ I_{x,3}, I_{y,3} &: \text{quadrupolar order and double quantum} \\ I_{x,3} + I_{y,3} = -I_{z,3}, I_{z,2} &: \text{double quantum} \\ I_{z,1} &: \text{Zeeman order} \\ I_{x,3} - I_{y,3} &: \text{quadrupolar order} \end{aligned}$$

In the following, we express the density operator by the above fictitious spin-$\frac{1}{2}$ operators and assume an ensemble of spin $I = 1$ nuclei in a large, static magnetic field. In this situation, the spin system is subject to the secular part of the first order quadrupolar interaction as well as a possible resonance offset. In the rotating frame the Hamiltonian is

$$H = H_{RF} + H_{int} \tag{2}$$

with

$$\begin{aligned} H_{int} &= -\Delta I_z + \frac{1}{3}\omega_Q[3I_zI_z - I(I+1)] \\ &= -2\Delta I_{z,1} + \frac{2}{3}\omega_Q(I_{x,3} - I_{y,3}) \end{aligned} \tag{3}$$

$$\omega_Q = \frac{3e^2qQ}{4I(2I-1)\hbar}\frac{[3\cos^2\theta - 1 + \eta\sin^2\theta\cos 2\varphi]}{2} \tag{4}$$

where Δ is the resonance offset, e^2qQ/h is the quadrupolar coupling constant, η is the asymmetry parameter and θ and φ are the usual Euler angles with respect to the azimuthal axis [11]. We will use the notation $\omega_{Q,0}$ to distinguish with ω_Q

$$\omega_{Q,0} = \frac{3e^2qQ}{4I(2I-1)\hbar} \tag{5}$$

which is half the observed splitting of a single crystal doublet when $\theta = 0$, or equal to the distance between the peaks in a Pake pattern when $\eta = 0$. Neglecting relaxation processes the time evolution of the density matrix is

$$\rho(t) = U\rho(0)U^{-1} \tag{6}$$

with

$$U = \exp(-iHt) \tag{7}$$

where H is time independent. In what follows, the initial density matrix $\rho(0)$ is taken as $\rho(0) = I_z$. The observable signal is determined by computing

$$Sig = \mathrm{Tr}(\rho \cdot R_{\pm y}) \tag{8}$$

where the operator for the receiver, $R_{\pm y}$, is defined as $R_\pm \equiv \pm I_{y,1} \mp iI_{x,1}$.

Before highlighting the effects of various errors on the alignment echo three-pulse sequence, we will show that the phase cycling scheme given in Table 1 (from reference [3]) eliminates double quantum coherence under ideal experimental conditions. In Table 1, ϕ_i and ϕ_r represent the phases of the ith pulse and receiver, respectively. In the discussion that follows, $\rho^n(t)$ represents the density operator for the nth step of the phase cycle given in Table 1. For ideal experimental conditions we assume the experiment is performed on-resonance, thus $\Delta = 0$ in Eq. (3). The propagator for an RF pulse with flip angle β and phase ϕ according to Eq. (7) is

$$U_{RF}(\beta,\phi) = \exp(-i\beta 2I_\phi) \tag{9}$$

where $\beta = \pi/2$ for the first pulse and $\beta = \pi/4$ for the second and last pulses. The factor of 2 in the spin rotation propagator comes from the definition of the fictitious spin-$\frac{1}{2}$ operators. For the computations that follow we assume $\tau = \frac{\pi}{2\omega_Q}$ for maximum conversion to quadrupolar order and will expand on this assumption in the proceeding section. By using Eqs. (3), (6), (7) and (9) the various states of the spin system at $t = \tau + T_-$ for each step of the four-step phase cycling are

$$\rho^{1,2}(\tau + T_-) = Q(I_{x,3} - I_{y,3})/2 + D(I_{y,3} + I_{x,3})/2 \tag{10a}$$

$$\rho^{3,4}(\tau + T_-) = Q(I_{x,3} - I_{y,3})/2 - D(I_{x,3} + I_{y,3})/2 \tag{10b}$$

In the above expressions, $Q = D = 1$. The symbols Q and D have been inserted as coefficients to label the quadrupolar ordered term and double quantum coherence terms respectively. These labels show the presence and magnitude of different quantum coherence created after the second delay T, and will be used to track their evolution into detectable signals in the remaining steps of the pulse sequence. It is important to note that the pulse sequence even in the absence of artifacts creates double quantum coherence. Follow-

Table 1
A four-step phase cycling scheme for suppressing double quantum coherence in quadrupolar alignment echo spectroscopy [3]. The phases ϕ_1, ϕ_2, ϕ_3 and ϕ_r refer to the three pulses and receiver phase in the pulse sequence shown in Fig. 1.

Step no.	ϕ_1	ϕ_2	ϕ_3	ϕ_r
1	x	y	y	y
2	x	y	$\bar{y}$	$\bar{y}$
3	$\bar{y}$	x	y	y
4	$\bar{y}$	x	$\bar{y}$	$\bar{y}$

ing the last pulse, the signals at $2\tau + T$ for each step of the phase cycle are

$$Sig^{1,2}(2\tau + T) = 1/8(-D - 3Q) \tag{11a}$$

$$Sig^{3,4}(2\tau + T) = 1/8(D - 3Q) \tag{11b}$$

In the above expressions the superscripts denote each step of the phase cycle in Table 1. The signal after phase cycling is thus

$$Sig(2\tau + T) = \sum_{i=1}^{4} Sig^{i}(2\tau + T) = (-3/2)Q \tag{12}$$

The result of this computation demonstrates that the four-step phase cycling scheme given in Table 1 cancels double quantum coherence entirely and that the detected signal results only from the quadrupolar ordered state. In the four subsections below we describe the effect of various pulse errors as well as off-resonance effects. It will be shown that these errors may introduce extra terms, such as single quantum coherence and Zeeman order in the intermittent states. Without proper phase cycling, some of these terms may be transformed into an observable signal. However, with the four-step phase cycling scheme given in Table 1, to a good approximation, all terms other than quadrupolar order are suppressed in the detected signal. For the case of a flip error, finite pulse width effect and pulse transient we assume an on-resonance condition with $\Delta = 0$ in Eq. (3).

2.1. Flip error

For the case of a pulse flip error, where the flip angle of any given pulse deviates from a perfect rotation, we study the possible leakage of various multiple quanta in the detected signal. The propagator for the RF pulse with a flip error is modeled as

$$U_{RF}(\beta, \phi; \delta_\beta) = \exp[-i(\beta + \delta_\beta)2I_\phi] \tag{13}$$

In the above expression δ_β is the flip error for a pulse with flip angle β. For the $\pi/4$ pulses the error δ_{45} is taken to be half of that of the $\pi/2$ pulse, δ_{90}. The phase of each pulse in the cycle, ϕ, is again listed in Table 1. Using this model and the procedure described above, the various states of the spin system at time $\tau + T_-$ for each step of the phase cycling are

$$\rho^{1,2}(\tau + T_-) = \frac{I_{y,3} - I_{x,3}}{2}Q + \frac{I_{y,3} + I_{x,3}}{2}D - I_{z,1}Z - I_{y,2}S_4 - I_{y,1}S_3 - I_{x,1}S_1 - I_{x,2}S_2 \tag{14a}$$

$$\rho^{3,4}(\tau + T_-) = -\frac{I_{x,3} - I_{y,3}}{2}Q - \frac{I_{x,3} + I_{y,3}}{2}D - I_{z,1}Z + I_{x,2}S_4 - I_{x,1}S_3 + I_{y,1}S_1 - I_{y,2}S_2 \tag{14b}$$

where

$$\begin{aligned} Q &= D = \cos^2(\delta_{90}) \\ Z &= \cos\frac{1}{4}(\pi + 2\delta_{90}) \\ S_1 &= \cos(T\omega_Q)\sin\delta_{90}\sin\frac{1}{4}(\pi + 2\delta_{90}) \\ S_2 &= \sin(T\omega_Q)\sin\delta_{90}\sin\frac{1}{4}(\pi + 2\delta_{90}) \\ S_3 &= \frac{1}{2}\sin(T\omega_Q)\sin 2\delta_{90} \\ S_4 &= \frac{1}{2}\cos(T\omega_Q)\sin 2\delta_{90} \end{aligned} \tag{15}$$

In the above expressions Q denotes quadrupolar order, D denotes double quantum coherence, Z denotes Zeeman order, and S_1, S_2, S_3, S_4 all denote single quantum coherence. Following the third pulse the signals detected at $t = T + 2\tau$ for each step of the phase cycling are

$$\begin{aligned} Sig^1(2\tau + T) &= \frac{1}{8}\Big[-(D + 3Q)\cos(\delta_{90}) - 4iS_2\cos\frac{1}{4}(\pi + 2\delta_{90}) + 4S_4\sin(\delta_{90})\Big] \\ Sig^2(2\tau + T) &= \frac{1}{8}\Big[-(D + 3Q)\cos(\delta_{90}) + 4iS_2\cos\frac{1}{4}(\pi + 2\delta_{90}) - 4S_4\sin(\delta_{90})\Big] \\ Sig^3(2\tau + T) &= \frac{1}{8}\Big[(D - 3Q)\cos(\delta_{90}) + 4iS_4\cos\frac{1}{4}(\pi + 2\delta_{90}) + 4S_2\sin(\delta_{90})\Big] \\ Sig^4(2\tau + T) &= \frac{1}{8}\Big[(D - 3Q)\cos(\delta_{90}) - 4iS_4\cos\frac{1}{4}(\pi + 2\delta_{90}) - 4S_2\sin(\delta_{90})\Big] \end{aligned} \tag{16}$$

and the signal after phase cycling is

$$Sig(2\tau + T) = \sum_{i=1}^{4} Sig^{i}(2\tau + T) = -\frac{3}{2}Q\cos\delta_{90} \tag{17}$$

From the above expressions it is clear that Zeeman order (labeled by Z) which appears at time $t = \tau + T_-$ in Eqs. (14a) and (14b) does not contribute to the phase cycled signal in Eq. (17); the first two steps of the phase cycling are able to cancel single quantum coherence (labeled S_2 and S_4). Together with the last two steps of the phase cycling scheme, double quantum coherence (labeled D) is also canceled. The only term which is created and detected is the quadrupolar ordered term (labeled Q). Thus, the computation shows that even in the presence of a pulse flip error there is no leakage of quantum coherence and one only detects quadrupolar order after phase cycling. The final detected signal is real and is amplitude modulated by $\cos^3(\delta_{90})$. Note that when the error $\delta_{90} = 0$ we find that the results agree with the situation of no error, given in Eq. (12). The signal intensity as a function of the $\pi/2$ flip angle error, δ_{90}, in the range of 0–10° is plotted in Fig. 2. The figure shows that the relative reduction of the signal intensity is less then 5% when the flip error is as large as 10°. The pulse flip error may be experimentally measured by a flip–flip sequence [12].

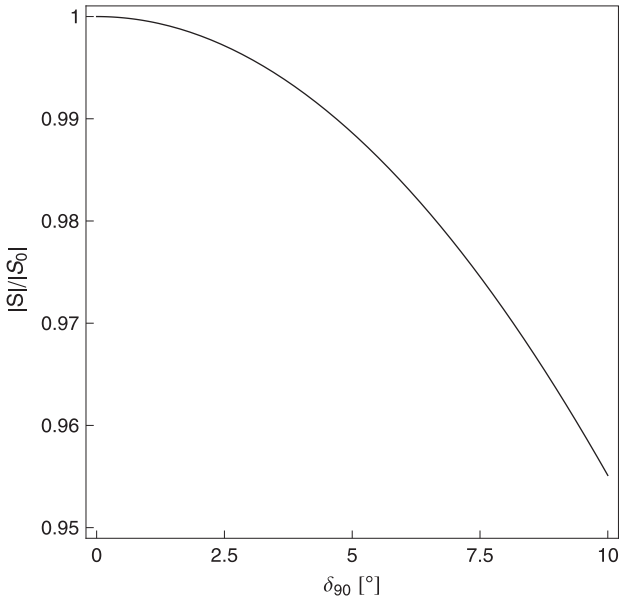

Fig. 2. Absolute value of the alignment echo intensity at $t = 2\tau + T$ with errors (S) divided by the signal intensity without errors (S_0) as a function of the pulse flip error measured in degrees, δ_{90}.

2.2. Finite pulse width effects

In the situation of a rigid solid, the quadrupolar coupling constant for the deuteron can be as large as 200 kHz and therefore the evolution under the quadrupolar interaction during the RF pulses cannot be ignored. The propagator for an RF pulse of width t_p thus includes the quadrupolar interaction,

$$U_{RF}(\beta,\phi;t_p) = \exp[-i(\beta 2I_\phi + H_{int}t_p)] \tag{18}$$

In the following we assume that $\omega_Q t_p$ is a small quantity. This assumption is justified under the conditions where the $\pi/2$ pulse width t_p is on the order of 1 to 3 μs, and the quadrupolar frequency $\omega_Q/2\pi$ is less than 20 kHz, so that $\omega_Q t_p \leqslant 0.12\pi < \pi/2$. We have performed a Taylor expansion of the solution to second order of this small quantity to simplify the complex algebraic expressions and give insight into the dynamics of the spin system in the presence of this error. Following the evolution under the sequence of pulses and delays shown in Fig. 1, one obtains the following density matrices before the last pulse for each step of the phase cycle

$$\rho^{1,2}(\tau+T_-) = -I_{x,1}S_1 + I_{x,2}S_2 + I_{y,1}S_3 - I_{y,2}S_4 + I_{z,1}Z_1 - I_{z,2}D_2 - \frac{I_{y,3}-I_{x,3}}{2}Q - \frac{I_{y,3}+I_{x,3}}{2}D_1 \tag{19a}$$

$$\rho^{3,4}(\tau+T_-) = I_{y,1}S_1 + I_{y,2}S_2 + I_{x,1}S_3 + I_{x,2}S_4 + I_{z,1}Z_1 + I_{z,2}D_2 + \frac{I_{x,3}-I_{y,3}}{2}Q + \frac{I_{x,3}+I_{y,3}}{2}D_1 \tag{19b}$$

where

$$\begin{aligned} Q = D_1 &= \frac{-8\pi^2 + (8+\pi(4+\pi))\omega_Q^2 t_p^2}{8\pi^2} \\ D_2 &= \frac{\omega_Q t_p}{\sqrt{2}\pi} \\ Z_1 &= \frac{\omega_Q^2 t_p^2}{\sqrt{2}\pi^2} \\ S_1 &= \frac{\omega_Q t_p \sin(T\omega_Q)}{\sqrt{2}\pi} \\ S_2 &= \frac{\omega_Q t_p \cos(T\omega_Q)}{\sqrt{2}\pi} \\ S_3 &= \frac{4\pi(2+\pi)\omega_Q t_p \cos(T\omega_Q) - 6\pi\omega_Q^2 t_p^2 \sin(T\omega_Q)}{8\pi^2} \\ S_4 &= \frac{6\pi\omega_Q^2 t_p^2 \cos(T\omega_Q) + 4\pi(2+\pi)\omega_Q t_p \sin(T\omega_Q)}{8\pi^2} \end{aligned} \tag{20}$$

Again, the symbols Q and D_1 indicate the magnitude of quadrupolar order and double quantum coherence respectively, S_1, S_2, S_3 and S_4 denote single quantum coherence and Z_1 denotes Zeeman order. In addition, the term D_2 is a second double quantum coherence term created due to finite pulse width effects.

Upon implementing the four-step phase cycling scheme again given in Table 1, the detected signal at $t = 2\tau + T$ is given by

$$\begin{aligned} Sig(2\tau+T) &= \mathrm{Tr}\left(\sum_{i=1}^{4}\rho^i(T+2\tau)\cdot R_i\right) \\ &\approx \frac{1}{4}\left[i\sqrt{2}\omega_Q Z_1 t_p + Q\left(6 - \frac{3\omega_Q^2 t_p^2}{\pi^2}\right)\right] \\ &\approx \frac{3}{16}\left[-8 + \frac{(12+4\pi+\pi^2)(\omega_Q t_p)^2}{\pi^2}\right] \end{aligned} \tag{21}$$

The result shows that when finite pulse widths are taken into account the detected signal contains Zeeman order as well as quadrupolar order. However, the Zeeman order contribution to the signal intensity is cubic in t_p and can be ignored to second order. The quadrupolar order contribution to the signal intensity decreases as the pulse width increases, and is plotted in Fig. 3 as a function of the pulse width t_p for several values of the quadrupolar frequency $\omega_Q/2\pi$ from 2 kHz to 20 kHz. The figure highlights that the relative reduction of the signal intensity is less than 5% for the largest value of $\omega_Q t_p$ we considered, $\omega_Q\, t_p/2\pi = 0.06$.

2.3. Anti-symmetric transients

In this section we model the effects of RF transients. In a previous work [13], we adopted a model after A. J. Vega [14], where any RF pulse of our pulse sequence includes a transient effect. The model consists of an orthogonal RF field that is applied to the spin system before and after the main pulse. The propagator for an anti-symmetric pulse transient is given by

$$U_{RF}(\beta,\phi;\alpha_t) = \exp\left(-i\alpha_t 2I^t_{\phi+\pi/2}\right) \times \exp(-i\beta 2I_\phi) \times \exp\left(i\alpha_t 2I^t_{\phi+\pi/2}\right) \tag{22}$$

where the first and last propagators represent a pulse transient that rotate the ensemble by an angle α_t and have phases orthogonal to that of the main pulse. For example, if the main pulse is about the x-axis then the transient is about the + y-axis before and - y-axis after the pulse. We performed a computation that accounts for pulse transients on all pulses in the spin alignment sequence, assuming that the transient flip angle α_t is the same for all pulses. Because α_t will typically be small relative to the main pulse duration we have taken a Taylor expansion to second order in our density matrix calculation. The states of the spin system before the last pulse for each step of the phase cycling are

$$\rho^{1,2}(\tau+T_-) = I_{x,1}S_1 + I_{x,2}S_2 + I_{y,1}S_3 + I_{y,2}S_4 + I_{z,1}Z_1 - I_{z,2}D_2 - \frac{I_{y,3}-I_{x,3}}{2}Q + \frac{I_{y,3}+I_{x,3}}{2}D_1 \tag{23a}$$

$$\rho^{3,4}(\tau+T_-) = -I_{y,1}S_1 + I_{y,2}S_2 + I_{x,1}S_3 - I_{x,2}S_4 + I_{z,1}Z_1 + I_{z,2}D_2 + \frac{I_{x,3}-I_{y,3}}{2}Q - \frac{I_{x,3}+I_{y,3}}{2}D_1 \tag{23b}$$

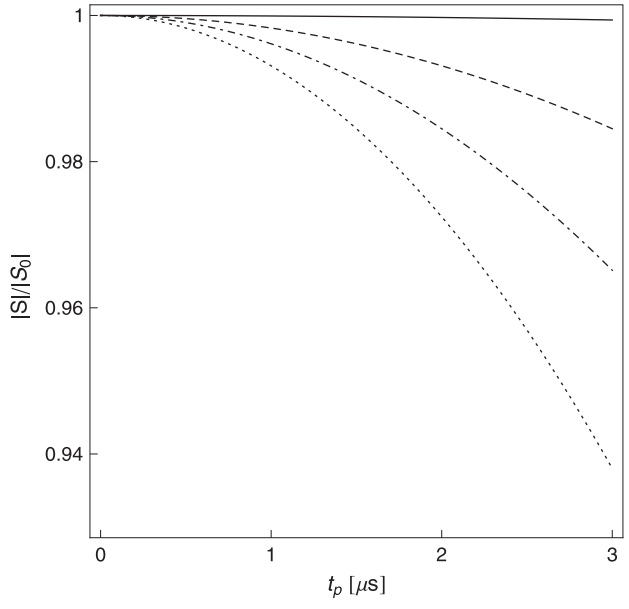

Fig. 3. Absolute value of the alignment echo intensity at $t = 2\tau + T$ with errors (S) divided by the signal intensity without errors (S_0) as a function of the $\pi/2$ pulse width t_p in units of μs for four values of the quadrupolar frequency ω_Q. The notation in the figure is as follows: solid line $\omega_Q/2\pi = 2$ kHz, dashed line $\omega_Q/2\pi = 10$ kHz, dotdashed line $\omega_Q/2\pi = 15$ kHz and dotted line $\omega_Q/2\pi = 20$ kHz.

where

$$
\begin{aligned}
Q &= \alpha_t^2 - 1 \\
D_1 &= 1 - 3\alpha_t^2 \\
D_2 &= \sqrt{2}\alpha_t \\
Z_1 &= \frac{\alpha_t^2}{\sqrt{2}} \\
S_1 &= \frac{1}{2}\left(\sqrt{2}\alpha_t^2\cos(T\omega_Q) + 2\alpha_t\sin(T\omega_Q)\right) \\
S_2 &= \frac{1}{2}\left(-2\alpha_t\cos(T\omega_Q) + \sqrt{2}\alpha_t^2\sin(T\omega_Q)\right) \\
S_3 &= \left(-1+\sqrt{2}\right)\alpha_t^2\sin(T\omega_Q) \\
S_4 &= \left(-1+\sqrt{2}\right)\alpha_t^2\cos(T\omega_Q)
\end{aligned}
\tag{24}
$$

The notation again for the various symbols Q, D_1, S_1,S_2, S_3, S_4 and Z_1, D_2 are the same as those in the previous section on finite pulse errors. The computation shows the creation of single quantum coherence, double quantum coherence and Zeeman order in addition to the quadrupolar order terms resulting from RF transients. After implementing the four-step phase cycling one obtains the following expression for the signal at $t = 2\tau + T$

$$
\begin{aligned}
Sig(2\tau+T) &= \mathrm{Tr}\left(\sum_{i=1}^{4}\rho^i(T+2\tau)\cdot R_i\right) \\
&\approx \frac{3}{4}Q\left[2 - 2i\left(-1+\sqrt{2}\right)\alpha_t + \left(-3+2\sqrt{2}\right)\alpha_t^2\right] \\
&\approx -\frac{3}{2} + \frac{3}{2}i\left(-1+\sqrt{2}\right)\alpha_t + \left(\frac{15}{4} - \frac{3}{\sqrt{2}}\right)\alpha_t^2
\end{aligned}
\tag{25}
$$

The result shows that the detected signal in the presence of RF transients arises only from the quadrupolar ordered state. However, the detected signal contains both real and imaginary components whose individual amplitudes depend on the transient flip angle α_t. The real part and the magnitude of the complex signal as functions of α_t in the range of 0–30° are plotted in Fig. 4. When the flip angle of the RF transient is as large as 30° the signal intensity on the real channel reduces to approximately 70%, and the magnitude of the complex signal reduces to approximately 75% of the signal intensity under ideal conditions. Experimentally RF transients may be characterized by a flip–flop sequence by measuring the modulation frequency induced by the transient [12,15]. From average Hamiltonian theory, the first order term of Magnus expansion for our transient model in the flip-flop sequence is

$$
H_T^0 = J_1/\tau_c(I_{z,1} - I_{y,1}) \tag{26}
$$

where τ_c is cycle time of the multiple pulse sequence and the modulation induced by the RF transient in a stroboscopic measurement is given by [13]

$$
\omega = -\sqrt{2}J_1/\tau_c. \tag{27}
$$

The relation between J_1 and the transient flip angle α_t in our model is

$$
J_1 = -\alpha_t \tag{28}
$$

2.4. B_z offset

Lastly we consider the case when the internal Hamiltonian has a nonzero resonance offset, i.e. $\Delta \neq 0$ in Eq. (3). We assume the propagators for the RF pulses are the same as that for the ideal condition given in Eq. (9). The density matrices at $t = \tau + T_-$ for the various steps in the phase cycling are

$$
\begin{aligned}
\rho^{1,2}(\tau+T_-) = &-I_{x,2}S_4 + I_{x,1}S_3 - I_{y,2}S_2 - I_{y,1}S_1 - I_{z,2}D_2 \\
&- \frac{I_{x,3} - I_{y,3}}{2}Q + \frac{I_{x,3} + I_{y,3}}{2}D_1
\end{aligned}
\tag{29a}
$$

$$
\begin{aligned}
\rho^{3,4}(\tau+T_-) = &-I_{y,2}S_4 - I_{y,1}S_3 + I_{x,2}S_2 - I_{x,1}S_1 + I_{z,2}D_2 \\
&- \frac{I_{x,3} - I_{y,3}}{2}Q - \frac{I_{x,3} + I_{y,3}}{2}D_1
\end{aligned}
\tag{29b}
$$

where

$$
\begin{aligned}
Q &= \cos\left(\frac{\pi\Delta}{2\omega_Q}\right) \\
D_1 &= \cos(2T\Delta)\cos\left(\frac{\pi\Delta}{2\omega_Q}\right) - \sqrt{2}\sin(2T\Delta)\sin\left(\frac{\pi\Delta}{2\omega_Q}\right) \\
D_2 &= \frac{1}{2}\left[\cos\left(\frac{\pi\Delta}{2\omega_Q}\right)\sin(2T\Delta) + \sqrt{2}\cos(2T\Delta)\sin\left(\frac{\pi\Delta}{2\omega_Q}\right)\right] \\
S_1 &= \frac{\sin(T\omega_Q)\sin(T\Delta)\sin\left(\frac{\pi\Delta}{2\omega_Q}\right)}{\sqrt{2}} \\
S_2 &= \frac{\cos(T\omega_Q)\sin(T\Delta)\sin\left(\frac{\pi\Delta}{2\omega_Q}\right)}{\sqrt{2}} \\
S_3 &= \frac{\cos(T\Delta)\sin(T\omega_Q)\sin\left(\frac{\pi\Delta}{2\omega_Q}\right)}{\sqrt{2}} \\
S_4 &= \frac{\cos(T\omega_Q)\cos(T\Delta)\sin\left(\frac{\pi\Delta}{2\omega_Q}\right)}{\sqrt{2}}
\end{aligned}
\tag{30}
$$

With the four-step phase cycling the final detected signal is

$$
Sig(2\tau+T) = \mathrm{Tr}\left(\sum_{i=1}^{4}\rho^i(T+2\tau)\cdot R_i\right) = -\frac{3}{2}e^{-\frac{i\pi\Delta}{2\omega_Q}}Q \tag{32}
$$

The above result shows that in the presence of a resonance offset that the detected signal still only arises from quadrupolar order with no additional quantum coherence leaked into the detected signal. There are two observed effects that the resonance offset error has on the signal; there is a phase and amplitude modulation of the signal that is proportional to Δ/ω_Q. Because the resonance offset

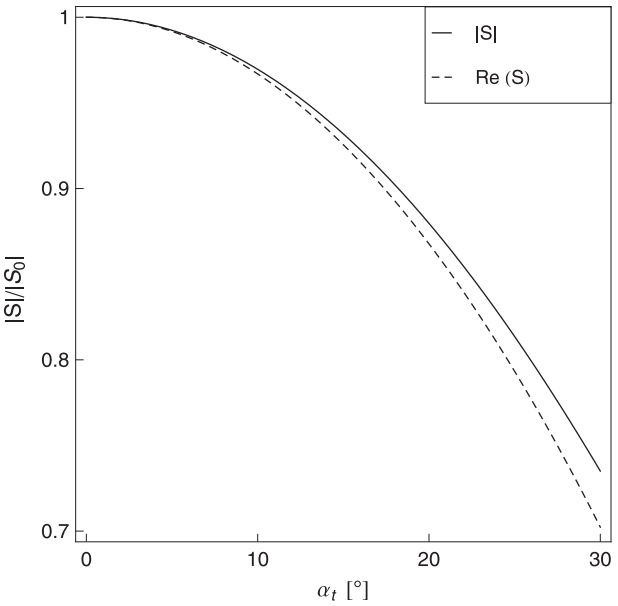

Fig. 4. Absolute value of the alignment echo intensity at $t = 2\tau + T$ with errors (S) divided by the signal intensity without errors (S_0) as a function of the transient flip angle α_t in degrees. The dashed line represents the real component of the signal and the solid line represents the magnitude of the signal.

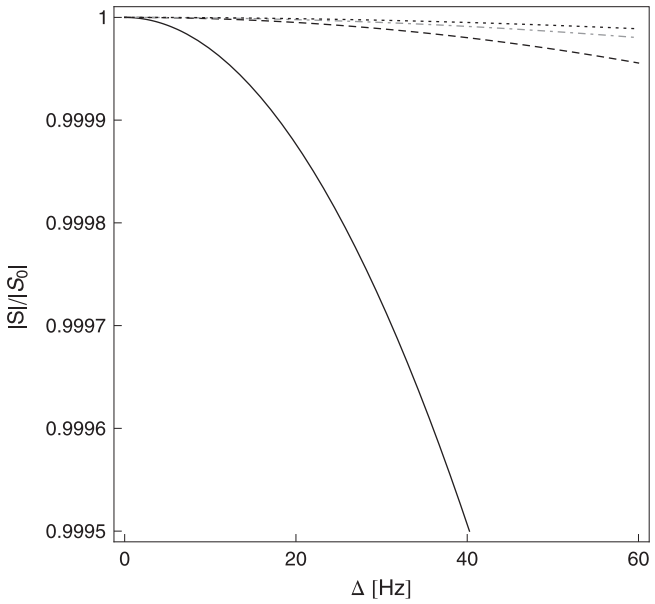

Fig. 5. Absolute value of the alignment echo intensity at $t = 2\tau + T$ with errors (S) divided by the signal intensity without errors (S_0) as a function of the resonance offset Δ for four values of the quadrupolar frequency ω_Q. The notation in the figure is as follows: solid line $\omega_Q/2\pi = 2$ kHz, dashed line $\omega_Q/2\pi = 10$ kHz, dotdashed line $\omega_Q/2\pi = 15$ kHz and dotted line $\omega_Q/2\pi = 20$ kHz.

is typically much smaller than the quadrupolar frequency, the effect on the detected signal is negligible. Fig. 5 highlights the variation in the amplitude of the signal as a function of the resonance offset for four different values of quadrupolar frequencies, $\omega_Q/2\pi$, from 2 kHz to 20 kHz. The results show the reduction in signal in the alignment echo amplitude in the presence of an off-resonance effect as large as 40 Hz is negligible for quadrupolar frequencies $\omega_Q/2\pi = 20$ kHz.

3. Case II: Simulations of alignment echo powder line shapes in the presence of pulse errors

In the previous section the analysis was performed for a single value of ω_Q and the delay τ was set such that $\tau = \pi/2\omega_Q$. Under these conditions, it is straightforward to show that one achieves optimal conversion to quadrupolar order under ideal experimental conditions. For situations where there is more than one quadrupolar frequency, such as in the case of polycrystal or powdered samples, the above condition cannot be achieved and it is challenging to obtain analytical expressions for a distribution of ω_Q. In this section, we consider simulation results that illustrate the effects of a given pulse error on the alignment echo spectra acquired by the three-pulse sequence. Broadband excitation of quadrupolar spectra may be achieved by composite pulses and alleviate the stringent requirement that $\tau = \pi/2\omega_Q$ to some extent, but are not the subject of this work [16–18]. The parameters we used in the simulation are $\omega_{Q,0}/2\pi = 64$ kHz, $\eta = 0$ with $\tau = 25$ μs or $\tau = 30$ μs. For each value of τ, the spectra for three types of errors were individually investigated. The simulations are performed using a home written algorithm in MATLAB and the error models described in the previous section. In all of our simulations we considered 360 powder averages, $T = 100$ μs, a 350 μs acquisition window and a dwell time of 0.5 μs. The spectra shown in Figs. 6 and 7 are obtained with a Gaussian broadening of 2 kHz and zero padding the data once.

Figs. 6 and 7 show the simulated FID and spectra for $\tau = 25$ μs and $\tau = 30$ μs respectively under various pulse error conditions. It should be noted that the vertical scale of the spectra shown in Fig. 6 is half that in Fig. 7. Referring to Fig. 6b one observes that the effect of a flip error is to introduce an asymmetry into the

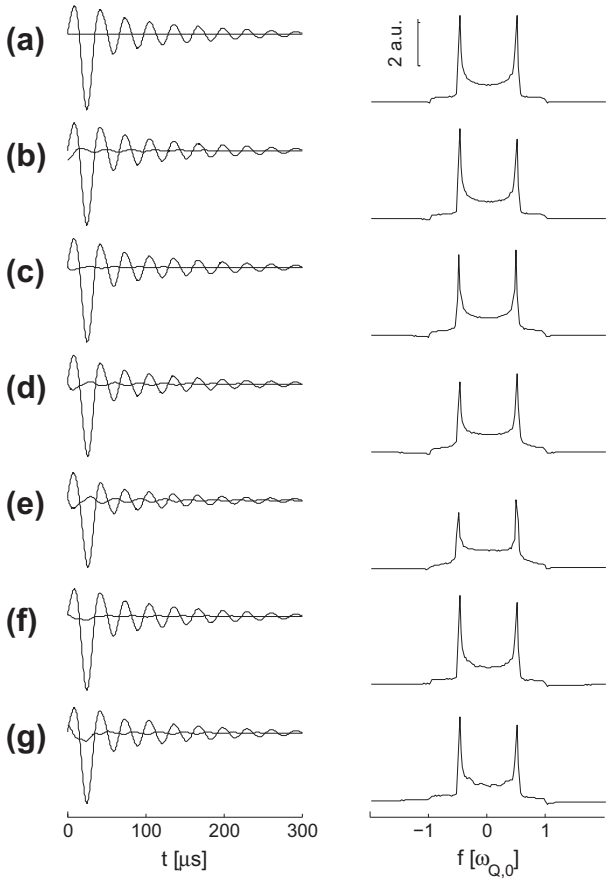

Fig. 6. Simulated phase cycled alignment echo FID and the corresponding real component of the spectra for the case of $\tau = 25$ μs (other parameters are provided in the text). (a) Ideal experimental conditions. (b) A flip error with $\delta_\beta = 6°$. (c) A 90° pulse of width equal to 1 μs. (d) A 90° pulse of width 2 μs. (e) A 90° pulse of width 3 μs. (f) A pulse transient with flip angle $\alpha_t = 9°$. (g) A pulse transient with flip angle $\alpha_t = 18°$.

spectra. A finite pulse width effect, shown in Fig. 6c–e, in the range of 1–3 μs reduces the signal intensity and introduces an asymmetry in the spectra as well. Fig. 6f and g show results for two different RF transients. The main effect of an RF transient in addition to causing an asymmetry distortion is that it introduces some additional artifacts in the center of the spectra, and as the transient is made larger this feature becomes more pronounced. With the introduction of any of the three errors we modeled, an imaginary component is introduced in the FID.

Fig. 7, highlights results for $\tau = 30$ μs; the data demonstrate that the effects of the various errors appear to be larger than when $\tau = 25$ μs. The effect of a flip error shown in Fig. 7b also introduces an asymmetry in the spectra, but to a greater extent than that of Fig. 6b where $\tau = 25$ μs. The effect of a finite pulse width, shown in Fig. 7c–e also distorts the spectra, but to a greater extent than that shown in the results of Fig. 6c–e. RF transients still result in a spectral distortion in the center of the spectra, however, the asymmetry appears to be much greater than the condition when $\tau = 25$ μs shown in Fig. 6f and g. Together, the simulations show that the spectral distortions due to pulse errors may be minimized, to some extent, by judiciously choosing the time between the first two pulses.

An intuitive method of choosing the optimal value of τ is to consider the maxima of the function

$$\int_0^\pi sin^2\left(\omega_{Q,0}\frac{3\cos^2\theta - 1}{2}\tau\right)sin(\theta)d\theta \tag{33}$$

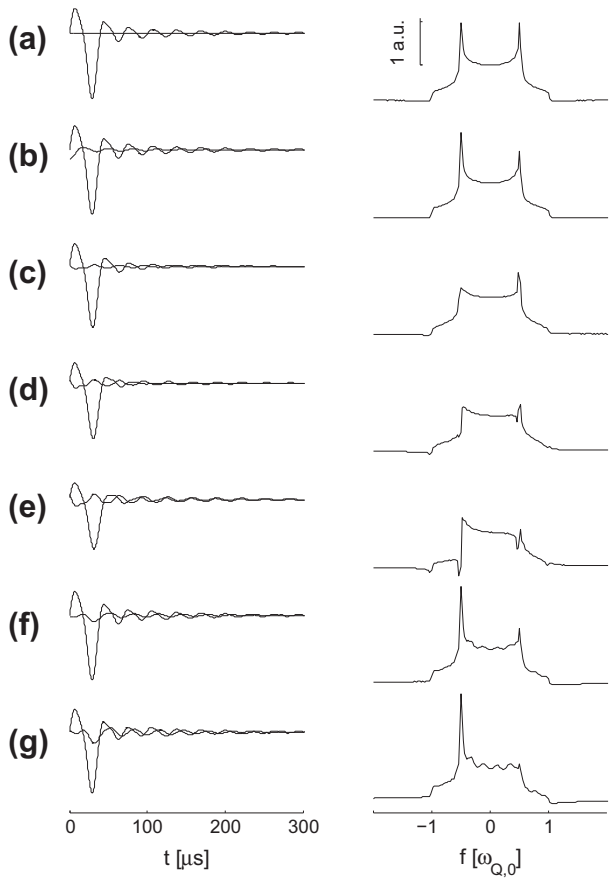

Fig. 7. Simulated phase cycled alignment echo FID and the corresponding real component of the spectra for the case of $\tau = 30$ μs (other parameters are provided in the text). (a) Ideal experimental conditions (b) A flip error with $\delta_\beta = 6°$. (c) A 90° pulse of width equal to 1 μs. (d) A 90° pulse of width 2 μs. (e) A 90° pulse of width 3 μs. (f) A pulse transient with flip angle $\alpha_t = 9°$. (g) A pulse transient with flip angle $\alpha_t = 18°$.

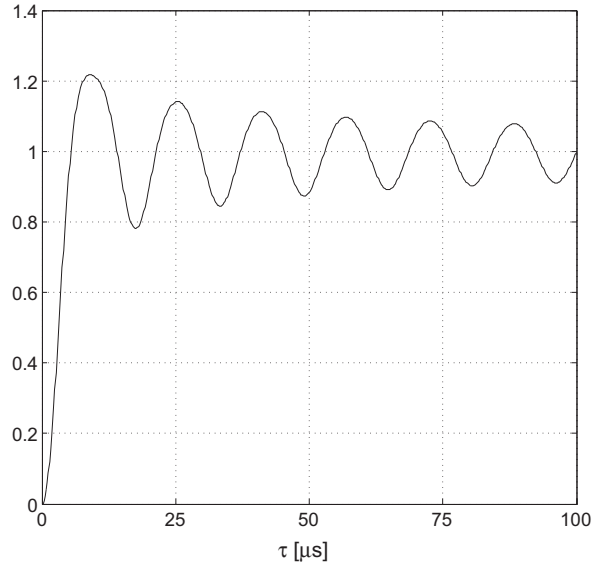

Fig. 8. Plot of the function shown in Eq. (33) versus τ for the case $\omega_{Q,0}/2\pi = 64$ kHz and $\eta = 0$.

which is the powder average of the prefactor of the signal intensity, under ideal conditions. To be clear, the $sin^2\left(\omega_{Q,0}\frac{3\cos^2\theta-1}{2}\tau\right)$ amplitude modulation arises from the generation and subsequent readout of quadrupolar order. A graph of this function is shown in Fig. 8 for the case $\omega_{Q,0}/2\pi = 64$ kHz. Referring to the figure, it is evident that the optimal choice for τ is approximately 9 μs. Other than a reduction in signal intensity, the spectra simulated with this choice of τ essentially reproduced that shown for the next maximum, $\tau = 25$ μs. While the shorter τ choice may maximize the conversion to quadrupolar order, this choice may result in additional distortions in the acquired spectra due to instrumental dead times and probe ring down effects in experiments. Further, Fig. 8 accounts for the observation that the signal intensity at $\tau = 30$ μs is smaller than that at $\tau = 25$ μs, as the shorter choice in τ allows for more efficient conversion of single quantum coherence to quadrupolar alignment with the $\pi/4$ pulse. In practice one may measure the value of ω_Q and η with a solid echo and generate a similar figure for determining an optimal choice in τ.

4. Experimental

We performed a measurement of the quadrupolar alignment relaxation rate on powdered samples of perdeuterated hexamethylbenzene (HMB) and polyethelene (PE). We measured $\omega_{Q,0}/2\pi = 16.1$ kHz in the HMB sample and $\omega_{Q,0}/2\pi = 120.5$ kHz in the PE sample. The ^{2}H NMR signals were obtained at 27.55 MHz, using a Tecmag Apollo solid state NMR system and a home-built NMR probe. The pulse length was 2.8 μs for the $\pi/2$ pulse with τ set to 35 μs in all our experiments. In signal averaging, 80 scans were accumulated for the HMB sample and 1000 scans were accumulated for the PE sample with a recycle delay of 2 s. All the experiments were performed at room temperature. In order to probe the effectiveness of the suppression of double quantum coherence we implemented the four-step phase cycling scheme in Table 1 as well as a two step phase cycling scheme consisting of the first two steps in Table 1; the later scheme suppresses single quantum coherence but not double quantum coherence. The integrated spectral intensity as a function of the delay T are shown in Fig. 9 for HMB and Fig. 10 for PE, on a logarithmic scale to reveal the details of the short time behavior. The purpose of the experimental data presented is to demonstrate the efficacy of the four-step phase cycling scheme under real experimental conditions and verify some of the results of our analysis.

Data for the HBM sample using the two-step phase cycling scheme was fitted by two exponentials, shown as the solid line through the triangle points, with time constants 57.5 ms and 0.5 ms. The four-step phase cycled data, however, is well fit by a single exponential and the fit is shown as the solid line through the circle points, with a time constant of 57.5 ms. It is clear that the 0.5 ms fast decay component from the two-step phase cycling scheme is double quantum coherence. The absence of other components needed to fit both data sets suggest that there is no single quantum coherence or Zeeman order leakage under our experimental conditions. Furthermore, the four-step phase cycled data indicate that there is no double quantum coherence or other terms that are leaked into the detected signal other than the quadrupolar ordered state by using this scheme. Experimental data acquired on PE are highlighted in Fig. 10 and demonstrate similar results as that found on HMB. Data acquired with two step phase cycling scheme are shown as triangle points; the fit shown as a solid line includes three time constants: 147.7 ms, 3.8 ms and 0.09 ms. Using the four step phase cycling scheme we observe only two time constants: 147.7 ms and 3.8 ms. The double quantum signal that has a decay time constant of 0.09 ms observed in the two step phase cycling experiment is suppressed in the four step phase cycling experiment. It is evident that the pulse phase cycling scheme is also robust for this sample that has a quadrupolar frequency

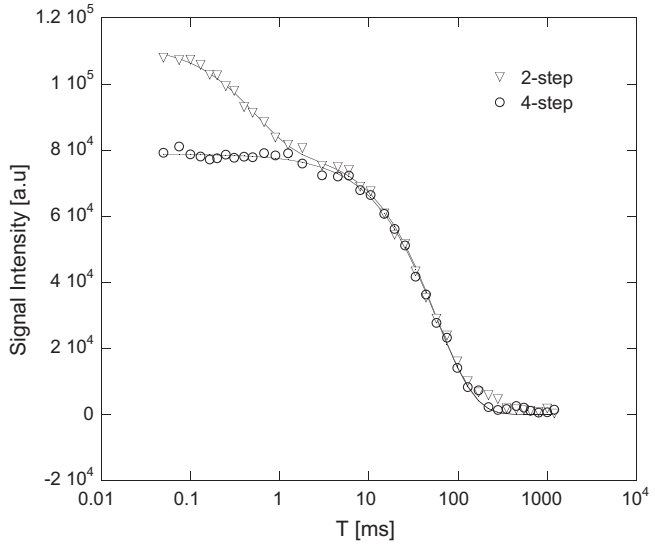

Fig. 9. Results from relaxation measurements shown on a logarithmic scale (in time) for two different phase cycling schemes in powdered perdeuterated hexamethylbenzene. As discussed in the text, the two step phase cycling scheme allows for detection of double quantum coherence simultaneously with the quadrupolar alignment signal. The four-step phase cycling scheme suppresses double quantum coherence and allows for detecting the quadrupolar alignment signal only, in the absence of experimental artifacts. In the figure the experimental data are shown as open points and the best fits are shown as solid lines. The error bars are approximately 4%.

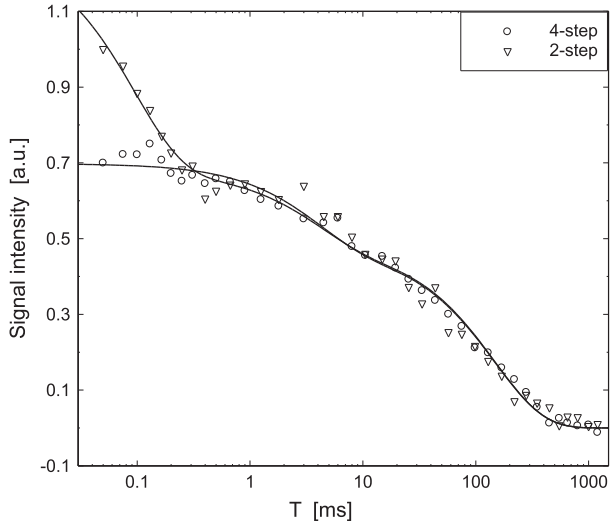

Fig. 10. Results from relaxation measurements shown on a logarithmic scale (in time) for two different phase cycling schemes in deuterated polyethylene. As discussed in the text, the two step phase cycling scheme allows for detection of double quantum coherence simultaneously with the quadrupolar alignment signal. The four-step phase cycling scheme suppresses double quantum coherence and allows for detecting the quadrupolar alignment signal only, in the absence of experimental artifacts. In the figure the experimental data are shown as open points and the best fits are shown as solid lines. The error bars are approximately 4%.

approximately 7.4 times larger than the HMB sample. The bi-exponential decay in the spin alignment echo experiment of PE has been previously studied by Speiss and coworkers, and is attributed to 'rigid' and 'mobile' deuterons in crystalline and amorphous regions of the polymer [19]. In our experimental setup, we estimated the pulse flip errors and transients with flip-flip and flip-flop pulse sequences [12]. The flip error for the 90° pulse in our system was determined to be approximately 3.5° and the pulse transient flip angle was determined to be approximately 11°. While an 11° degree phase transient is within the limits of our Taylor expansion computed in the previous section, we found that the phase cycling scheme was robust in suppressing unwanted double quantum coherence. While the pulse flip error was 3.5°, the analysis showed that the four-step phase cycling scheme is also robust against this error and suppresses unwanted double quantum coherence when $\omega_Q\tau = \pi/2$. Finally, in our experimental setup $\omega_Q t_p \ll \pi/2$, so no double quantum or single quantum or Zeeman order leakage is expected to be realized, when $\omega_Q\tau = \pi/2$. We note that the experimental artifacts commonly encountered in other systems may be greater than that found on our system, and it behooves the experimenter to consider running two separate experiments with two separate phase cycles to verify that the short time decay in T_{1Q} experiments is indeed quadrupolar order.

5. Conclusion

In this work we report on the effects of a variety of experimental imperfections on spin $I = 1$ quadrupolar alignment echo spectroscopy. We studied the potential leakage of unwanted quantum coherence as well as the reduction in signal intensity for four different types of commonly encountered experimental artifacts. For the case of a single quadrupolar frequency (in the case of a single crystal), the findings indicate that by implementing a well known four-step phase cycling scheme that pulse flip errors, finite pulse width effects, RF transients and off-resonance effects will not introduce unwanted quantum coherences. Off-resonance effects have the smallest effect and are negligible in many rigid or semi-rigid solids. Pulse flip errors and RF transients reduce the signal intensity for typical experimental errors to a similar extent. Finite pulse width effects may have substantial effects if the quadrupolar interaction is large, resulting in a reduction in signal intensity comparable in magnitude to the effects of the pulse flip errors and transients. We studied the various artifacts that may arise in the situation of a powder distribution, via simulation. The artifacts associated with the pulse errors may be minimized to some extent by a judicious choice in τ, where single quantum coherence is maximally converted to quadrupolar order. Lastly, it is demonstrated experimentally that the potential leakage of double quantum coherence in the short time decay of quadrupolar alignment relaxation studies may be probed by performing two separate experiments; one cycle that intentionally allows for detecting the double quantum signal and a second cycle that only allows for detecting quadrupolar order.

Acknowledgments

G.S. Boutis acknowledges support from the Professional Staff Congress of the City University of New York and NIH Grant No. 7SC1GM086268-03. The content is solely the responsibility of the authors and does not necessarily represent the official views of the National Institute of General Medical Sciences or the National Institutes of Health.

References

[1] H. Spiess, Molecular dynamics of solid polymers as revealed by deuteron NMR, Colloid Polym. Sci. 261 (3) (1983) 193–209.
[2] H. Spiess, Deuteron spin alignment: a probe for studying ultraslow motions in solids and solid polymers, J. Chem. Phys. 72 (1980) 6755.
[3] R. Vold, W. Dickerson, R. Vold, Application of the Jeener–Broekaert pulse sequence to molecular dynamics studies in liquid crystals, J. Magn. Res. 43 (1981) 213–223.
[4] M. Lausch, H. Spiess, Ultraslow tetrahedral jumps in solid hexamethylenetetramine studied by deuteron spin alignment, Chem. Phys. Lett. 71 (1980) 182–186.
[5] R. Prosser, J. Davis, Dynamics of an integral membrane peptide: a deuterium NMR relaxation study of gramicidin, Biophys. J. 66 (1994) 1429–1440.

[6] M. Hatcher, D. Mattiello, G. Meints, J. Orban, G. Drobny, A solid-state deuterium NMR study of the localized dynamics at the C9pG10 step in the DNA Dodecamer [d (CGCGAATTCGCG)] 2, J. Am. Chem. Soc. 120 (1998) 9850–9862.
[7] G. Olsen, M. Bardaro, D. Echodu, G. Drobny, G. Varani, Hydration dependent dynamics in RNA, J. BioMol. NMR 45 (2009) 133–142.
[8] G. Bodenhausen, H. Kogler, R. Ernst, Selection of coherence-transfer pathways in NMR pulse experiments, J. Magn. Res. 58 (1984) 370–388. 1969.
[9] A. Jerschow, Nonideal rotations in nuclear magnetic resonance: estimation of coherence transfer leakage, J. Chem. Phys. 113 (2000) 979–986.
[10] S. Vega, A. Pines, Operator formalism for double quantum NMR, J. Chem. Phys. 66 (1977) 5624–5644.
[11] A. Abragam, The Principles of Nuclear Magnetism, Oxford University Press, USA, 1983.
[12] U. Haeberlen, in: Adv. Magn. Reson. (Suppl. 1), Academic, New York, 1976.
[13] C. Sun, G. Boutis, Simulation studies of instrumental artifacts on spin $I = 1$ double quantum filtered NMR spectroscopy, J. Magn. Res. 205 (2010) 102–108.
[14] A. Vega, Controlling the effects of pulse transients and RF inhomogeneity in phase-modulated multiple-pulse sequences for homonuclear decoupling in solid-state proton NMR, J. Magn. Res. 170 (2004) 22–41.
[15] W. Rhim, D. Elleman, L. Schreiber, R. Vaughan, Analysis of multiple pulse NMR in solids. II, J. Chem. Phys. 60 (1974) 4595–4604.
[16] S. Wimperis, G. Bodenhausen, Broadband excitation of quadrupolar order by modified Jeener–Broekaert sequences, Chem. Phys. Lett. 132 (1986) 194–199.
[17] S. Wimperis, Broadband and narrowband composite excitation sequences, J. Magn. Res. 86 (1990) 46–59. 1969.
[18] G. Hoatson, Broadband composite excitation sequences for creating quadrupolar order in 2H NMR, J. Magn. Res. 94 (1991) 152–159.
[19] D. Hentschel, H. Sillescu, H. Spiess, Deuteron nmr study of chain motion in solid polyethylene, Polymer 25 (8) (1984) 1078–1086.